Electronic Supplementary Material (ESI) for ChemComm.
This journal is © The Royal Society of Chemistry 2020

Supporting Information

Label-free homogeneous electrochemical cytosensor for ultrasensitive detection of cancer cells based on multiaptamer-functionalized DNA tetrahedral nanostructures

Limin Yang, Xuehan Yin, Panpan Gai, Feng Li*

College of Chemistry and Pharmaceutical Sciences, Qingdao Agricultural University, Qingdao 266109, People's Republic of China

* Corresponding author. E-mail: lifeng@qau.edu.cn (F. Li); Tel/Fax: +86-532-58957855.

Chemicals and Materials. Tris(hydroxymethyl)aminomethane (Tris), sodium chloride (NaCl) and magnesium chloride ($MgCl_2 \cdot 6H_2O$) were purchased from Sinopharm Chemical Reagent Co., Ltd. (Shanghai, China). 3-(4,5-dimethyl-thiazol-2-yl)-2,5-diph-enyltetrazolium bromide (MTT) was purchased from Aladdin Bio-Chem Technology Co., Ltd (Shanghai, China). GelRed was purchased from Solebo Biotechnology Co., Ltd. (Beijing, China). Indium tin oxide (ITO) glass was obtained from Shenzhen Nanbo Display Technology Co., Ltd. (Shenzhen, China). Fetal bovine serum (FBS), Dulbecco's modified Eagles medium (DMEM), and cell medium RPMI 1640 were obtained from Biological Industries Co., Ltd. (Beit-Haemek, Israel). The human breast cancer cell line MCF-7, human lung cancer cell line A549, human kidney cell line HEK 293T and human hepatocyte cell line HL-7702 were obtained from Procell Life Science Co., Ltd. (Wuhan, China). All reagents were of analytical pure. All specific sequences of ssDNA were prepared by Sangon Biotechnology Co., Ltd. (Shanghai, China). These sequences are displayed in Table S1. All aqueous solutions used in the experiments were prepared using ultrapure water, which was produced by a Milli-Q water purification system (Millipore).

Apparatus and Instrumentation. Nondenaturing polyacrylamide gels electrophoresis (PAGE), high resolution transmission electron microscopy (HRTEM) and atomic force microscope (AFM) were applied to investigate the formation of DNA tetrahedron nanoparticles. PAGE (8%) gel analysis was performed in 1 × TBE buffer (pH 7.9, 9 mM Tris-HCl, 9 mM boric acid, 0.2 mM EDTA) with 95 V for 1.5 h and stained for 20 min in a GelRed solution. The PAGE and gel imaging were conducted on Bio-Rad electrophoresis system and Gel Doc XR+ Imaging System (Bio-Rad Laboratories, Inc., U.S.A.), respectively. To characterize the morphology of the as-prepared DNA tetrahedron nanoparticles, the high-resolution transmission electron microscopy

(HRTEM) was performed with a Tecnai G² F30 (FEI, USA). For the AFM imaging, the sample was imaged on the AFM Multimode 8 (Bruker, Germany). Absorbance in the MTT assay was detected using microplate reader (Synergy 2, Biotek, USA). For the electrochemical analysis, the di□erential pulse voltammetric (DPV) measurements were carried out with a computer controlled Autolab electrochemical workstation (Metrohm, Netherlands) employing a three-electrode system: an indium tin oxide (ITO) working electrode with an active surface area of 0.12 cm^2, an Ag/AgCl reference electrode, and a platinum wire counter electrode. The ITO electrode was pretreated by ultrasonic treatment in ethanol and ultrapure water for 30 min, respectively, and then the ITO electrodes were put into 1 mM NaOH solution for 5 h, followed by sonication in ultrapure water for 10 min.

Preparation and characterization of DNA tetrahedron. DNA tetrahedral nanostructures were prepared by following the previously reported protocols. The designed strands were respectively dissolved in TM buffer (20 mM Tris, 50 mM $MgCl_2$, pH=8.0). For the preparation of aptamer-free DNA tetrahedral nanostructures, equimolar quantities of four strands (S1, S2, S3, S4) were mixed in TM buffer at a final concentration of 2.5 μM and heated to 95 °C for 10 min. Then, the mixture was rapidly cooled to 4 °C. The Apt-DTNs with various numbers of aptamer side chains were fabricated by mixing various sets of strands. The detail composition of Apt-DTNs was shown in Fig. S1**.** All the obtained tetrahedron solution was stored at 4 °C at least 6 h before the following experiments.

Cell culture. Human lung cancer cell line A549, human kidney cell line HEK 293T, and human hepatocyte cell line HL-7702 cells were cultured in DMEM. Human breast cancer cell line MCF-7 cells were cultured in RPMI 1640 medium. All cell lines were supplemented with 10% FBS and 1%

antibiotics penicillin/streptomycin. After the cells plated on chamber slides for 24 h, the cells were collected by centrifugation at 1000 rpm for 4 min and washed twice with buffer solution (10 mM Tris, 100 mM NaCl, pH=7.4). Subsequently, the cells were carefully diluted into the buffer solution with different concentrations. The cell number was counted by hemocytometer.

Cell cytotoxicity assay. MCF-7 cells were placed in 96-well microtiter plates. After attachment for 24 h, the cells were cultured with various concentrations of DTNs and Apt (II)-DTNs respectively. Afterward, 150 μL of MTT solutions (0.5 mg mL^{-1}) were introduced to each well. The MTT solution was removed after 4 h, and 200 μL of DMSO was added to each well. Absorbance was recorded at 490 nm.

Homogeneous electrochemical cancer cell detection. For cancer cell detection, the assay was performed in 100 μL of buffer (10 mM Tris-HCl, 100 mM NaCl, pH 7.4) containing 100 nM of Apt-TDNs, and target cancer cells (MCF-7 cells or A549 cells) with various concentrations. First, 100 nM of Apt-TDNs in buffer solution was incubated with the target cancer cells at 37 °C for 60 min. Then, the above mixture was treated by centrifugation at 1500 rpm for 5 min to eliminate cells and Apt-TDNs bound to the cell surface, and all the supernatant solution containing unbound Apt-TDNs was collected. Finally, a solution of MB (2 μM) was put into the above-obtained supernatant solution. The DPV measurements were performed from –0.3 to -0.1 V after 4 h 30 min. In the experiments for selectivity investigation, HL-7702 cells and HEK 293T cells were tested. To study the effect of the aptamer, the MCF-7 cells were pretreated with aptamer S2.2 (2 μM) for 1.0 h and then incubated with Apt (II)-DTNs (100 nM) 37 °C for another 1.0 h. Next, the same procedure was performed as mentioned above.

Figures

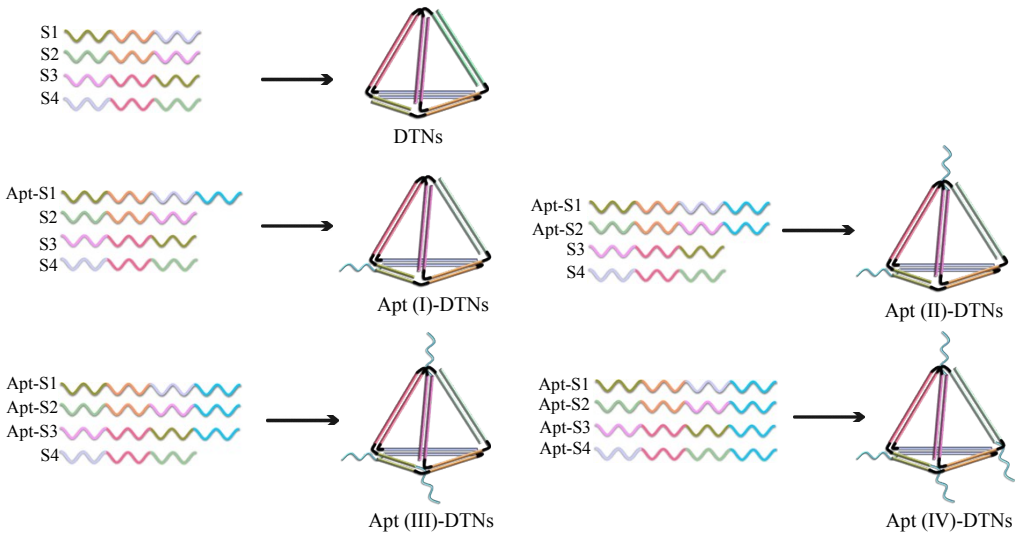

Fig. S1 Schematic illustration of the design of DTNs, and Apt-DTNs with 1 to 4 (I, II, III, IV) aptamer side chains.

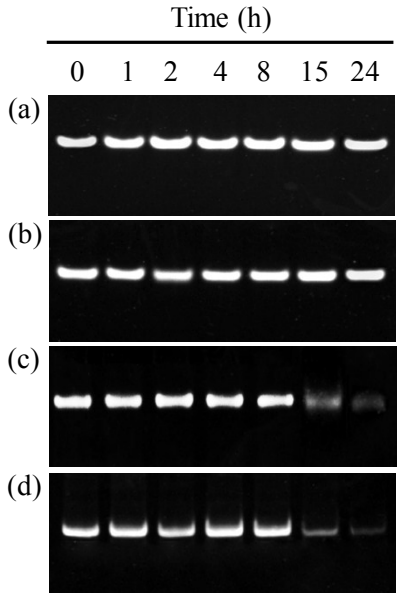

Fig. S2 Electrophoresis characterization of the stability of Apt-DTNs. Apt-DTNs (II) were incubated in Tris-HCl buffer (a), 1640 culture medium (b), Tris-HCl contained 10% FBS (c) and 1640 culture medium contained 10% FBS (d) with different time periods and then analyzed by using PAGE.

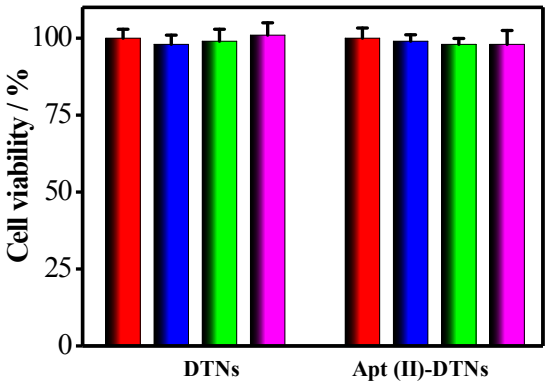

Fig. S3 Cell viability of MCF-7 cells incubated with different concentrations of DTNs and Apt (II)-DTNs for 24 h respectively. Red bars stand for the control, blue bars, green bars, and pink bars stand for 50 nM, 100 nM and 200 nM, respectively.

Cytotoxicity is an important factor before the application of Apt-DTNs-based platform in analysis of cancer cell. Therefore, a standard MTT assay was conducted on MCF-7 cells. The absorbance of MTT at 490 nm relies on the cell viability. The MCF-7 cells were incubated with DTNs or Apt (II)-DTNs with di□erent concentrations. Fig. S3 displayed that the cell viabilities were all over 90% when MCF-7 cells were incubated with DTNs and Apt (II)-DTNs with di□erent concentrations. The results indicated that these DNA nanostructures displayed little cytotoxicity or side effects in living cells, suggesting that they could be used as an approving candidate in cancer cell detection.

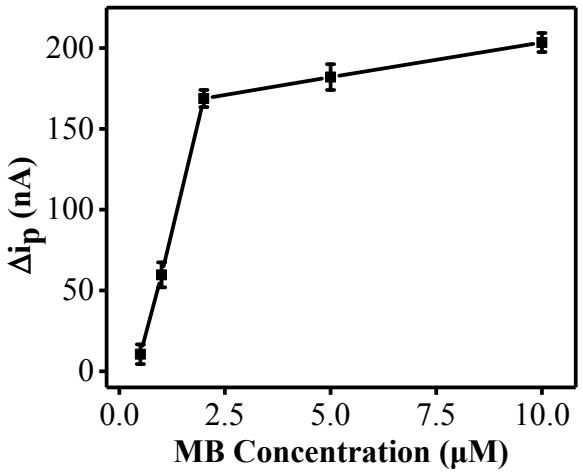

Fig. S4 The DPV peak current change Δi_p ($\Delta i_p = i_p - i_{p,0}$, in which i_p and $i_{p,0}$ are the DPV peak currents in the presence and absence of MCF-7 cells, respectively) versus the MB concentrations ranging from 0.5 μM to 10.0 μM. The concentration of Apt (II)-DTNs was 100 nM.

The influence of the MB concentration was studied by mixing of the different amount of MB with Apt (II)-DTNs. As shown in Fig. S4, the DPV peak current change Δi_p ($\Delta i_p = i_p - i_{p,0}$, in which i_p and $i_{p,0}$ are the DPV peak currents in the presence and absence of MCF-7 cells, respectively) was positively correlated with the MB concentration elevated from 0.5 μM to 2.0 μM, and which showed a slight increase when the MB concentration further increased to 10.0 μM (Fig. S3, ESI†), indicating that 2.0 μM of MB was the optimum concentration.

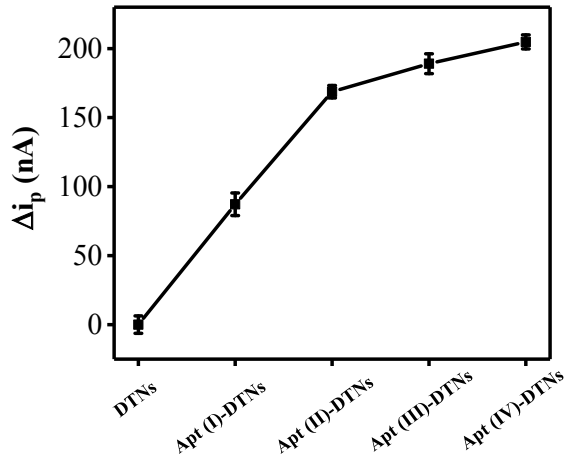

Fig. S5 DPV peak current change Δi_p ($\Delta i_p = i_p - i_{p,0}$, in which i_p and $i_{p,0}$ were the DPV peak currents in the presence and absence of MCF-7 cells respectively) versus the different kinds of tetrahedron nanostructures. The concentrations of MB, Apt (II)-DTNs and cell were 2.0 μM, 100 nM, and 1×10^5 cells mL^{-1} respectively.

To evaluate the impact of valence numbers of aptamer on tetrahedron in cancer cell detection, four kinds of Apt-DTNs were designed and studied. As shown in Fig S5, the DPV peak current change Δi_p were gradually enhanced when the valence number of aptamer motifs was increased to two, while having more than two aptamer ligands on one tetrahedron nanostructure did not clearly increase the current signal. It might be attributed to that fact that a certain local density of aptamer at one tetrahedron would significantly improve its targeting ability toward cancer cell, but it no longer increased when the number of aptamers was higher than this amount. Another possible reason was that one tetrahedron with high density of aptamer would occupy more binding sites of variable number of tandem repeatregions on MUC1, which affect other Apt-DTNs bound on cancer cells.

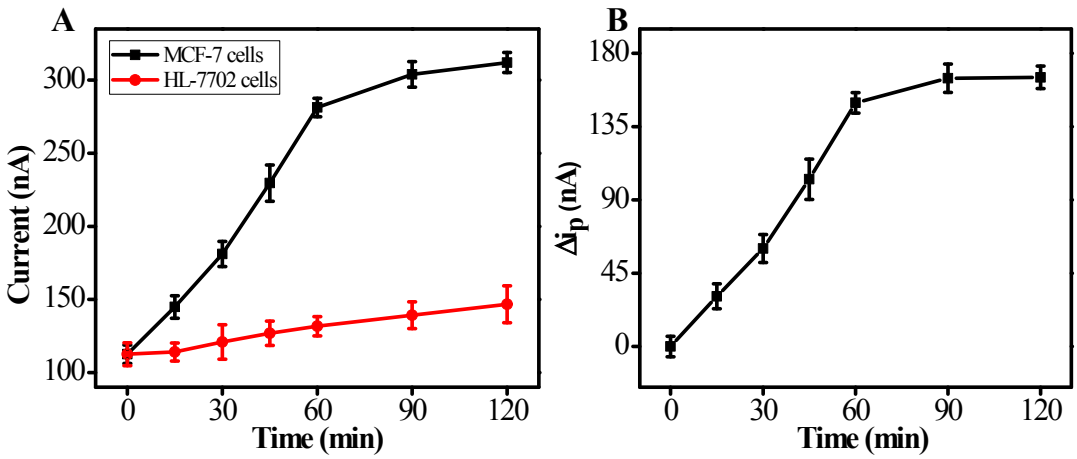

Fig. S6 (A) The DPV peak current of MB in the presence of MCF-7 cells and HL-7702 cells versus the incubation time respectively. (B) The DPV peak current change Δi_p ($\Delta i_p = i_{p,c} - i_{p,n}$, in which $i_{p,c}$ and $i_{p,n}$ were the DPV peak currents in the presence of MCF-7 cells and HL-7702 cells, respectively) versus the incubation time. The concentrations of MB, tetrahedron nanostructures and MCF-7 cells were 2 μM, 100 nM and 1×10^5 cells mL^{-1}, respectively.

The amount of the Apt-DTNs coupled with cancer cell surface was impacted by the incubation time before it reached thermodynamic equilibrium. Fig S6A showed the DPV signals of the MCF-7 and HL-7702 cells incubated with Apt (II)-DTNs at di□erent times. It was observed that the current signals of Apt (II)-DTNs-treated MCF-7 cells were progressively increased with the incubation time increased to 60 min, and then no obvious change was observed as the incubation time further extended from 60 min to 120 min. As a contrast, the changes of current signals in Apt (II)-DTNs-treated HL-7702 cells were always slightly raised from 0 to 120 min. Fig. S6B showed that the Δi_p increased progressively with the increase of reaction time and reached a plateau after 60 min, suggesting the optimal incubation time of 60 min for the subsequent studies.

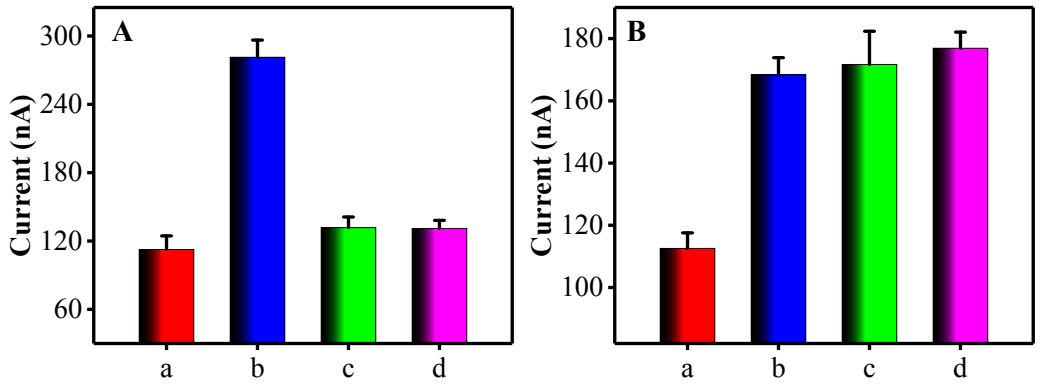

Fig. S7 Specificity analysis of the proposed cytosensor for detection of cancer cells. (A) Comparison of DPV peak currents in response to different types of cells: (a) blank, (b) MCF-7 cells, (c) HL-7702 cells, (d) HEK 293T cells. The concentrations of all groups of cells were 1×10^5 cells mL^{-1}. (B) Comparison of DPV peak currents in responses to MCF-7 cells (1×10^2 cells mL^{-1}) mixed with HL-7702 cells: (a) blank, (b) 1×10^2 MCF-7 cells mL^{-1}, (c) 1×10^2 MCF-7 cells mL^{-1} + 1×10^3 HL-7702 cells mL^{-1}, (d) 1×10^2 MCF-7 cells mL^{-1} + 1×10^4 HL-7702 cells mL^{-1}.

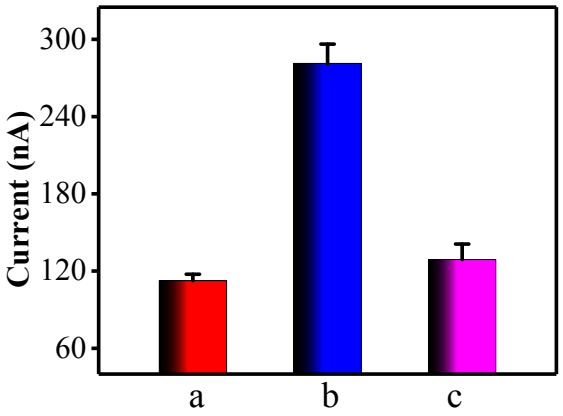

Fig. S8 DPV peak currents of the cytosensor under different conditions: (a) control, (b) MCF-7 cells, (c) MCF-7 cells + aptamer S2.2. The concentrations of the aptamer S2.2 and MCF-7 cells were 2.0 μM and 1×10^5 cells mL^{-1}, respectively.

The sensor good selectivity of Apt-DTNs-based for cancer cells can be attributed to the high affinity interaction of aptamer on tetrahedron toward the overexpressed MUC1 protein on cancer cell surface. To confirm this hypothesis, the MCF-7 cells were pretreated with the single strand aptamer S2.2 and then incubated with Apt (II)-DTNs. Fig. S8 showed that there was no significant change in current signal under this condition, validating the binding of aptamer S2.2 to MUC1 protein was indeed the key factor to achieve target cancer cell detection.

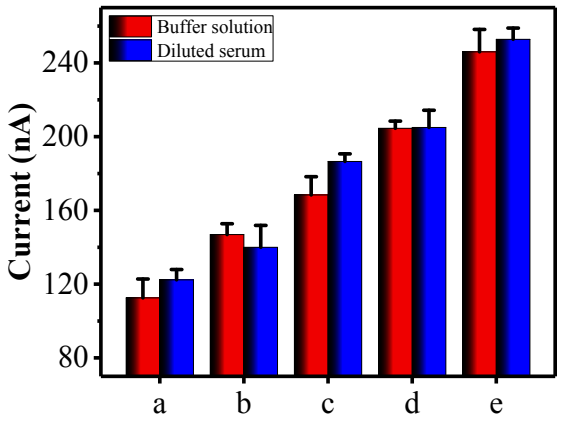

Fig. S9 DPV peak currents of the cytosensor in response to different concentration of MCF-7 cells in buffer solution (red bars) and diluted serum (blue bars). (a) 0, (b) 50, (c) 1×10^2, (d) 1×10^3 and (e) 1×10^4 cells mL^{-1} MCF-7 cells.

Table S1. Oligonucleotide sequences used in this work

Name	Sequence (form 5’ to 3’)
S1	ACATTCCTAAGTCTGAAACATTACAGCTTGCTACACGAGAAGAGCCGCCATAGTA
S2	TATCACCAGGCAATTGACAGTGTAGCAAGCTGTAATAGATGCGAGGGTCCAATAC
S3	TCAATTGCCTGGTGATAAAACGACACTACGTGGGAATCTACTATGGCGGCTCTTC
S4	TTCAGACTTAGGAATGTGCTTCCCACGTAGTGTCGTTTGTATTGGACCCTCGCAT
Apt-S1	GCAGTTGATCCTTTGGATACCCTGGTTTTTTTTACATTCCTAAGTCTGAAACATTACAGCTTGCTACACGAGAAGAGCCGCCATAGTA
Apt-S2	GCAGTTGATCCTTTGGATACCCTGGTTTTTTTTTATCACCAGGCAATTGACAGTGTAGCAAGCTGTAATAGATGCGAGGGTCCAATAC
Apt-S3	GCAGTTGATCCTTTGGATACCCTGGTTTTTTTTTCAATTGCCTGGTGATAAAACGACACTACGTGGGAATCTACTATGGCGGCTCTTC
Apt-S4	GCAGTTGATCCTTTGGATACCCTGGTTTTTTTTTTCAGACTTAGGAATGTGCTTCCCACGTAGTGTCGTTTGTATTGGACCCTCGCAT
aptamer S2.2	GCAGTTGATCCTTTGGATACCCTGG

Table S2. Comparison of the as-proposed strategy with other reported approaches

Method	Liner range (cells mL^{-1})	Detection limit	Refs.
Supersandwich cytosensor for selective and ultrasensitive detection of cancer cells using aptamer-DNA concatamer-quantum dots probes	1.0×10^2 - 1.0×10^6	50 cells mL^{-1}	1
Aptamer-DNA concatamer-quantum dots based electrochemical biosensing strategy for green and ultrasensitive detection of tumor cells via mercury-free anodic stripping voltammetry	1.0×10^2 - 1.0×10^7	60 cells mL^{-1}	2
Ultrasensitive and Selective Electrochemical Diagnosis of Breast Cancer Based on a Hydrazine-Au Nanoparticle-Aptamer Bioconjugate	50 - 2.0×10^4	26 cells mL^{-1}	3
Sensitive electrochemical aptamer cytosensor for highly specific detection of cancer cells based on the hybrid nanoelectrocatalysts and enzyme for signal amplification	1.0×10^2 - 1.0×10^7	15 cells mL^{-1}	4
Multiplex acute leukemia cytosensing using multifunctional hybrid electrochemical nanoprobes at a hierarchically nanoarchitectured electrode interface	5.0×10^2 - 1.0×10^7	350 cells mL^{-1}	5
Robust nonenzymatic hybrid nanoelectrocatalysts for signal amplification toward ultrasensitive electrochemical cytosensing	50 - 1.0×10^7	34 cells mL^{-1}, 42 cells mL^{-1}	6
A simple aptamer-functionalized gold nanorods based biosensor for the sensitive detection of MCF-7 breast cancer cells.	1.0×10^2 - 1.0×10^5	100 cells mL^{-1}	7
Near-Infrared Light-Driven Photoelectrochemical Aptasensor Based on the Upconversion Nanoparticles and TiO_2/CdTe Heterostructure for Detection of Cancer Cells.	1.0×10^3 - 1.0×10^5	400 cells mL^{-1}	8
Efficient Hydrogen-Generation CuO/Co_3O_4 Heterojunction Nanofibers for Sensitive Detection of Cancer Cells by Portable Pressure Meter	5.0×10^1-1.0×10^5	50 cells mL^{-1}	9
Reusable and dual-potential responses electrogenerated chemiluminescence biosensor for synchronously cytosensing and dynamic cell surface N-glycan evaluation	1×10^2 - 1×10^6	15 cells	10
Dual-target recognition sandwich assay based on core-shell magnetic mesoporous silica nanoparticles for sensitive detection of breast cancer cells	1×10^2 - 1×10^5	100 cells mL^{-1}	11
Construction of self-powered cytosensing device based on ZnO nanodisks@ g-C_3N_4 quantum dots and application in the detection of CCRF-CEM cells	20 - 2×10^4	20 cells mL^{-1}	12
Label-free homogeneous electrochemical cytosensor for ultrasensitive detection of cancer cells based on	50 - 1×10^6	5 cells	This work

multiaptamer-functionalized DNA tetrahedral nanostructures			

References

(1) Liu, H., Xu, S., He, Z., Deng, A., Zhu, J. J., 2013. Anal. Chem. 85, 3385–3392.

(2) Zheng, Y., Wang, X., He, S., Gao, Z., Di, Y., Lu, K., Li, K., Wang, J., 2019. 1 Biosens. Bioelectron. 26, 261–268.

(3) Zhu, Y., Chandra, P., Shim, Y. B., 2012. Anal. Chem. 85, 1058–1064.

(4) Sun, D., Lu, J., Zhong, Y., Yu, Y., Wang, Y., Zhang, B., Chen, Z., 2016. Biosens. Bioelectron. 75, 301–307.

(5) Zheng, T., Tan, T., Zhang, Q., Fu, J. J., Wu, J. J., Zhang, K., Zhu, J. J., Wang, H., 2013. Nanoscale 5, 10360–10368.

(6) Zheng, T., Zhang, Q., Feng, S., Zhu, J. J., Wang, Q., Wang, H., 2014. J. Am. Chem. Soc. 136, 2288–2291.

(7) Li, Y., Zhang, Y., Zhao, M., Zhou, Q., Wang, L., Wang, H., Wang, X., Zhan, L., 2016. Chem. Commun. 52, 3959–3961.

(8) Wang, K., Zhang, R., Sun, N., Li, X., Wang, J., Cao, Y., Pei, R., 2016. ACS applied materials & interfaces 8, 25834–25839.

(9) Ding, E., Hai, J., Li, T., Wu, J., Chen, F., Wen, Y., Wang, B., Lu, X., 2017. Anal. Chem. 89, 8140–8147.

(10) He, Y., Li, J., Liu, Y., 2015. Anal. Chem., 87, 9777–9785.

(11) Wang, W., Liu, S., Li, C., Wang, Y., Yan, C., 2018. Talanta, 182, 306–313.

(12) Pang, X., Cui, C., Su, M., Wang, Y., Wei, Q., Tan, W., 2018. Nano energy, 46, 101–109.